[PS]Depositional and Burial Domain Influences on Microporosity Modalities in Carbonaceous Mudstones of the Upper Cretaceous Colorado Group, Western Canada Foreland Basin*

Peng Jiang[1] and Burns A. Cheadle[1]

Search and Discovery Article #50802 (2013)**
Posted June 30, 2013

*Adapted from poster presentation given at AAPG 2013 Annual Convention and Exhibition, Pittsburgh, Pennsylvania, May 19-22, 2013
**AAPG©2013 Serial rights given by author. For all other rights contact author directly.

[1]Department of Earth Sciences, Western University, London, Ontario, Canada (bcheadle@uwo.ca)

Abstract

The fabric characteristics of intrinsic and secondary microporosity in carbonaceous mudstones provides insight into contrasting depositional and burial domain processes in the foredeep and back-bulge segments of a foreland basin. In particular, the relationship between disseminated organic matter and clay aggregates during deposition apparently influences the preservation of reactive kerogen as revealed by subsequent organic matter microporosity development during burial-related catagenesis. Laterally correlative strata spanning a foreland basin system offer the opportunity to evaluate how microfabric characteristics preserve evidence of distinct depositional and burial processes of different foreland basin segments.

The study is based on secondary electron and backscatter electron microscopy of 319 ion-milled cross-sectional surfaces from 43 samples. These samples are a representative gamut of Upper Cretaceous Colorado Group carbonaceous mudstones from thirteen cored wells spanning the Western Canada Foreland Basin (WCFB). Approximately 2600 SEM photomicrographs were acquired and evaluated in order to construct a comprehensive database of pore types. These fall into the broad categories of intercrystalline, intraparticle, organic matter and dissolution pores.

Understanding the relationship between organic matter porosity development and thermal maturity has been a principal focus of this work, with the intent to develop a generalized model for predictive purposes. The initial hypothesis posited a linear relationship between increasing thermal maturity and corresponding increase in organic matter microporosity in a transect from the back-bulge through the foredeep of the WCFB. The results, however, reveal very high degrees of spatial heterogeneity with respect to different modes of microporosity. This heterogeneity, in part, results from depositionally imposed modes of organic matter preservation and related advective transport of clay aggregates.

Depositional and Burial Domain Influences on Microporosity Modalities in Carbonaceous Mudstones of the Upper Cretaceous Colorado Group, Western Canada Foreland Basin

Peng Jiang[a*] and Burns A. Cheadle[a]
[a]Department of Earth Sciences, Western University, London, Ontario, Canada

1. Abstract

Fabric characteristics of intrinsic and secondary microporosity in carbonaceous mudstones provides insight into contrasting depositional and burial domain processes in the foredeep and back-bulge segments of a foreland basin. In particular, the relationship between disseminated organic matter and clay aggregates during deposition apparently influences the preservation of reactive kerogen as revealed by subsequent organic matter microporosity development during burial-related catagenesis. Laterally correlative strata spanning a foreland basin system offer the opportunity to evaluate how microfabric characteristics preserve evidence of distinct depositional and burial processes of different foreland basin segments.

The study is based on secondary electron and backscatter electron microscopy of 319 ion-milled cross-sectional surfaces from 43 samples. These samples are a representative gamut of Upper Cretaceous Colorado Group carbonaceous mudstones from thirteen cored wells spanning the Western Canada Foreland Basin (WCFB). Approximately 2600 SEM photomicrographs were acquired and evaluated in order to construct a comprehensive database of pore types. These fall into the broad categories of interparticle, intraparticle, organic matter, intercrystalline and dissolution pores.

Understanding the relationship between organic matter porosity development and thermal maturity has been a principal focus of this work, with the intent to develop a generalized model for predictive purposes. Our initial hypothesis posited a linear relationship between increasing thermal maturity and corresponding increase in organic matter microporosity in a transect from the back-bulge through the foredeep of the WCFB. The results, however, reveal very high degrees of spatial heterogeneity with respect to different modes of microporosity. This heterogeneity, in part, results from depositionally-imposed modes of organic matter preservation and related advective transport of clay aggregates.

This poster presents a progress report in which visual evidence is offered to support our working hypothesis regarding the profound influence of depositional microfabric on the ultimate reservoir characteristics of this particular self-sourcing stratal succession. Many questions remain, but the picture that is emerging for the Lower Colorado Group strongly suggests that the current rules of thumb regarding porosity development in carbonaceous mudstones require some critical re-evaluation.

2. Setting

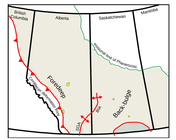

Our study area is the Western Canada Foreland Basin (WCFB) which developed during the Jurassic - Early Cretaceous Columbian Orogeny and Late Cretaceous to Paleogene Laramide Orogeny as a result of the collision and accretion of terranes on the western margin of the North American plate.
The WCFB has preserved foredeep, forebulge and backbulge segments (left) of the foreland basin that resulted from flexure of the North American plate and associated mantle dynamism. The Sweetgrass Arch (SGA) and Bow Island Arch (BIA) mark the approximate position of the forebulge although the location, timing and sense of motion on the forebulge were highly variable throughout the basin formation, influencing stratal packing and geometries.

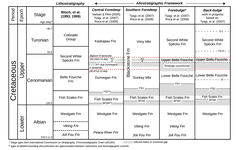

Our study focuses on the Cenomanian to Early Turonian Lower Colorado Group that brackets the second-order Greenhorn Transgression in the Western Interior Seaway. Bloch et al. (1993) established a lithostratigraphic subdivision of the Lower Colorado Group into the Second White Specks, Belle Fourche, Fish Scales and Westgate Formations. Our work extends the high-resolution allostratigraphic framework of Tyagi et al. (2007) from the WCFB foredeep eastward across the forebulge and into the backbulge segment of the basin (right). This approach will allow us to subdivide the stratal succession into time-equivalent packages with episodicities on the order of 100,000 to one million years.

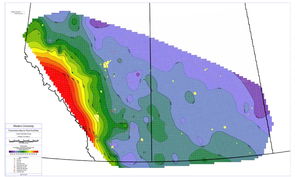

Our principal motivation is to understand how the carbonaceous mudstones of the Lower Colorado Group developed into several distinct self-sourcing (source-reservoir-seal) petroleum systems. In particular, our goal is to develop a petroleum system model for the liquids-rich Second White Specks oil play in western Alberta that incorporates an understanding of dynamic processes in the depositional and burial domains in order to bridge the gap between traditional petroleum systems modeling and reservoir characterization. In order to do so, we must build a foundation that combines high-resolution allostratigraphy with a deep understanding of the subsidence and thermal history of the basin. We begin from the perspective based on our regional compilation of Rock-Eval pyrolysis data that confirms the expected pattern of increasing thermal maturity, as expressed by increasing Rock-Eval Tmax (left) as the thickening Cretaceous stratal wedge filled the foredeep accommodation space.

3. Database

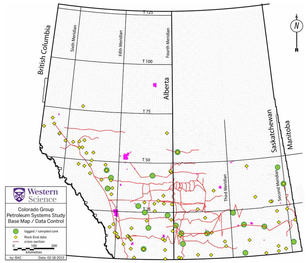

To date, 21 cores intersecting the Lower Colorado Group have been logged and sampled. The cores were selected based on well log characteristics, total interval and recovered core interval. The intent was to focus on cores that appear to preserve multiple allostratigraphic bounding surfaces within the interval of interest (based on log characteristics), with sufficient coverage to span the foredeep, forebulge, and backbulge segments of the WCFB.

In total, 417 samples have been collected from which 43 samples were identified as our initial FIB-SEM microscopy suite. A total of 319 surfaces were ion-milled on these samples, and 2607 images were digitally captured and archived for analysis.

Figure 3.1. Location map of the study area. The logged and sampled cores are indicated by the green dot symbols. Yellow diamond symbols indicate the locations of wells included in our regional Rock-Eval database for the Lower Colorado Group. Currently, 119 wells contribute to this database and we continue to add new control points. Each analysis in the database will be stratigraphically coded according to the high-resolution allostratigraphic framework that we are currently extending to the eastern edge of the WCFB. The major grid of cross-section lines is indicated in red.

4. Method

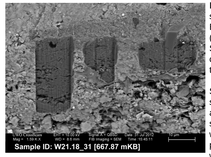

Imaging and pore characterization of a subset of the selected samples was conducted using the LEO (Zeiss) 1540XB Cross Beam Focused Ion Beam Scanning Electron Microscope (FIB/SEM) workstation in the Western Nanofabrication Facility. Samples were selected based on well log and Rock-Eval data characteristics, with the intent to sample a wide variety of rock types.

Small specimens (~1cmX1cmX5mm) were attached to aluminum stubs and coated with 5nm osmium tetroxide to reduce charging artifacts. After coating, samples were transferred into the SEM stage, and tilted to 54° for milling with a Ga+ ion beam. Millings were performed on the edge of freshly broken samples, and perpendicular to the bedding of the mudstones. Milled windows were typically 10 microns wide. Multiple windows were milled on each sample (left) to reduce sample bias.

Imaging was captured in the secondary electron (SE) and backscatter electron (BSE) detectors modes to capture topographical and compositional information, respectively. A limited number of energy-dispersive x-ray (EDX) scans were conducted to capture quantitative elemental data for confirmation of mineralogies.

Images were digitally captured and subsequently visually inspected in order to record microfabric characteristics and classify micropore types. Pore classification was done using the scheme developed by Loucks et al. (2012) (left). All observations, including qualitative assessment of relative abundances of pore types for each image and intensity of organic matter pore development were recorded in a database to create an archival reference for future investigations.

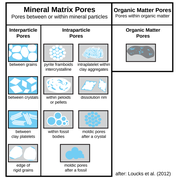

after: Loucks et al. (2012)

5. Mineral Matrix Pores

mineral species in photomicrographs: qz = quartz, cf - clay, py = pyrite, k = kerogen, cc = calcite

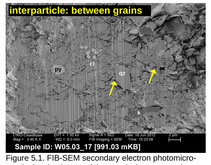

Figure 5.1. FIB-SEM secondary electron photomicrograph showing interparticle porosity between grains (yellow arrows).

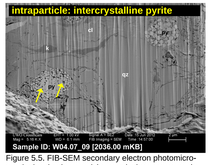

Figure 5.5. FIB-SEM secondary electron photomicrograph showing intraparticle porosity between crystals in a pyrite framboid (yellow arrows).

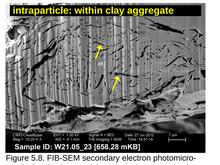

Figure 5.8. FIB-SEM secondary electron photomicrograph showing intraparticle porosity between platelets within a clay aggregate grain (yellow arrows).

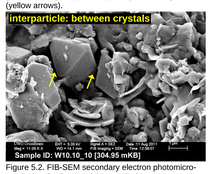

Figure 5.2. FIB-SEM secondary electron photomicrograph showing interparticle porosity between crystals (yellow arrows).

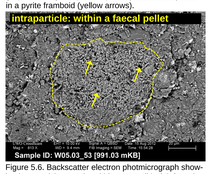

Figure 5.6. Backscatter electron photomicrograph showing intraparticle porosity within a coccolith-rich faecal pellet (yellow arrows).

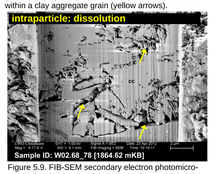

Figure 5.9. FIB-SEM secondary electron photomicrograph showing intraparticle porosity due to calcite dissolution (yellow arrows).

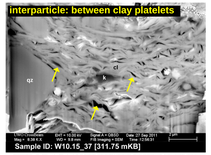

Figure 5.3. FIB-SEM backscatter electron photomicrograph showing interparticle porosity between clay platelets (yellow arrows).

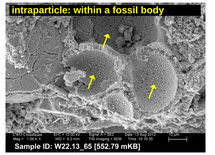

Figure 5.7. Secondary electron photomicrograph showing intraparticle porosity within the chambers of a foraminiferal test (yellow arrows). Note that the respiration pores represent a secondary form of the same class of porosity, albeit highly ineffective.

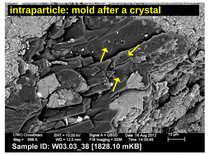

Figure 5.10. Backscatter electron photomicrograph showing intraparticle porosity due to molds after pyrite framboids imprinted on an inertinite maceral (yellow arrows). This is a rare, and ineffective, mode in the sample suite.

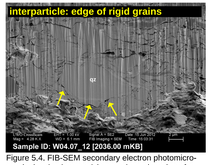

Figure 5.4. FIB-SEM secondary electron photomicrograph showing interparticle porosity at the edge of a rigid grain (yellow arrows).

Figures 5.1 through 5.10 show examples of the various modes of mineral matrix pores present in the carbonaceous mudstones of the Lower Colorado Group. Virtually every category of Loucks et al. (2012) classification scheme is represented within these diverse self-sourcing reservoirs. However, the pore types associated with clays (i.e.: Figures 5.3 and 5.8) are typically the most common mineral matrix pore. At the scale of observation of the ion-milled surfaces in these images (approximately 10 microns wide), the distinction between interparticle pores between clay platelets and intraparticle pores contained within clay aggregate grains can be enigmatic.
Intercrystalline pores within pyrite framboids (Figure 5.5), while not volumetrically significant, are commonly observed throughout the sample suite, regardless of basin position. Intraparticle pores within faecal pellets (Figure 5.6) are more common in the carbonate-rich facies of the backbulge basin.

6. Organic Matter (OM) Pores

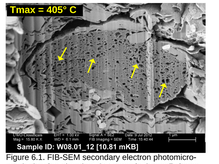

Figure 6.1. FIB-SEM secondary electron photomicrograph showing abundant OM pores in thermally immature amorphous kerogen (yellow arrows).

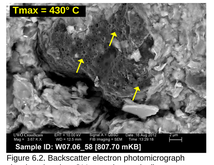

Figure 6.2. Backscatter electron photomicrograph showing abundant OM pores in marginally mature amorphous kerogen (yellow arrows).

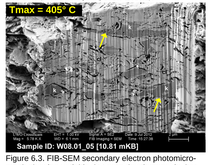

Figure 6.3. FIB-SEM secondary electron photomicrograph showing variable OM pore development in thermally immature amorphous kerogen (yellow arrows).

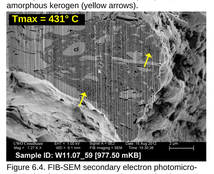

Figure 6.4. FIB-SEM secondary electron photomicrograph showing heterogeneous OM pore development (yellow arrows) in a clay-kerogen aggregate particle.

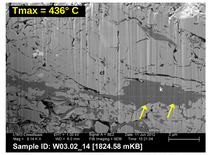

Figure 6.5. FIB-SEM secondary electron photomicrograph showing pinpoint OM pores (yellow arrows) in marginally mature amorphous kerogen.

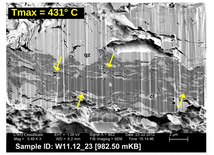

Figure 6.6. FIB-SEM secondary electron photomicrograph showing heterogeneous OM pore development (yellow arrows) associated with clay flakes.

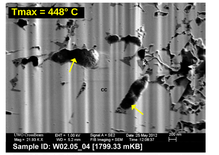

Figure 6.7. FIB-SEM secondary electron photomicrograph showing advanced stage of OM pore development (yellow arrows) in thermally mature kerogen.

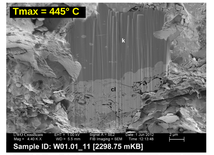

Figure 6.8. FIB-SEM secondary electron photomicrograph showing non-porous kerogen in a thermally mature sample.

Depositional and Burial Domain Influences on Microporosity Modalities in Carbonaceous Mudstones of the Upper Cretaceous Colorado Group, Western Canada Foreland Basin

Peng Jiang[a*] and Burns A. Cheadle[a]

[a]Department of Earth Sciences, Western University, London, Ontario, Canada

7. Clay Aggregates

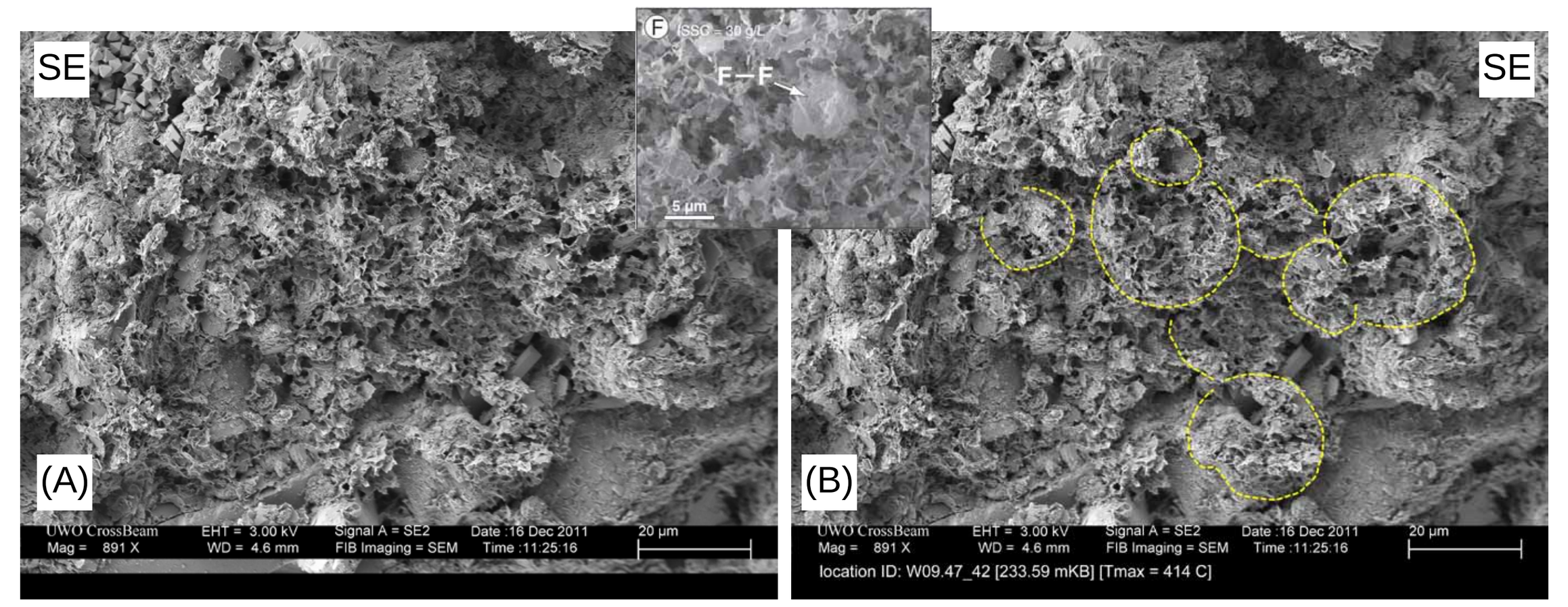

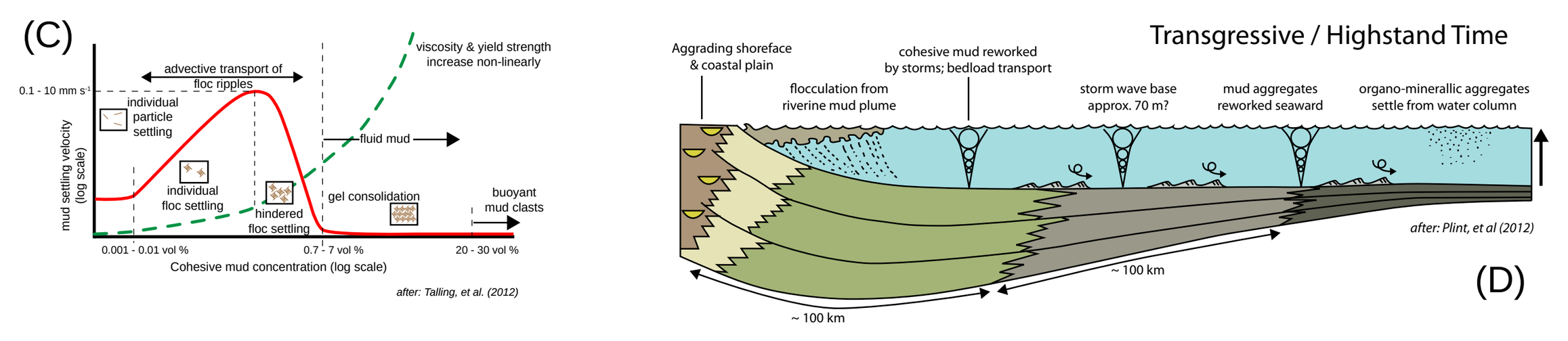

Figure 7.1. Secondary electron photomicrograph showing preservation of approximately spherical clay aggregate particles in a Lower Belle Fourche Alloformation sample from the eastern backbulge segment of the WCFB (location W09: sample depth 233.59 mKB). An uninterpreted image is shown in (A), and yellow dashed lines outline the perimeters of the aggregates in (B). The inset is a SEM image from Nishida et al. (2013) showing an experimentally-produced clay aggregate particle from a fluid mud simulation at a density of 30 g/L clay. The F-F label indicates the face-face clay platelet orientation that develops at high mud concentration, whereas the example from W09 exhibits the edge-face configuration that develops at slightly lower fluid mud concentrations.
The plot in (C), which is adapted from Talling et al. (2012), illustrates the transition of settling modes as a function of increasing mud concentration. The microfabrics preserved in the Lower Colorado Group samples from this study indicate intermediate concentrations close to the transition from hindered floc settling to gel consolidation characteristic of the onset of fluid mud transport.
We have interpreted these microfabrics as the result of wave-enhanced basinward reworking of cohesive mud and organominerallic aggregates in a shallow ramp setting (D).

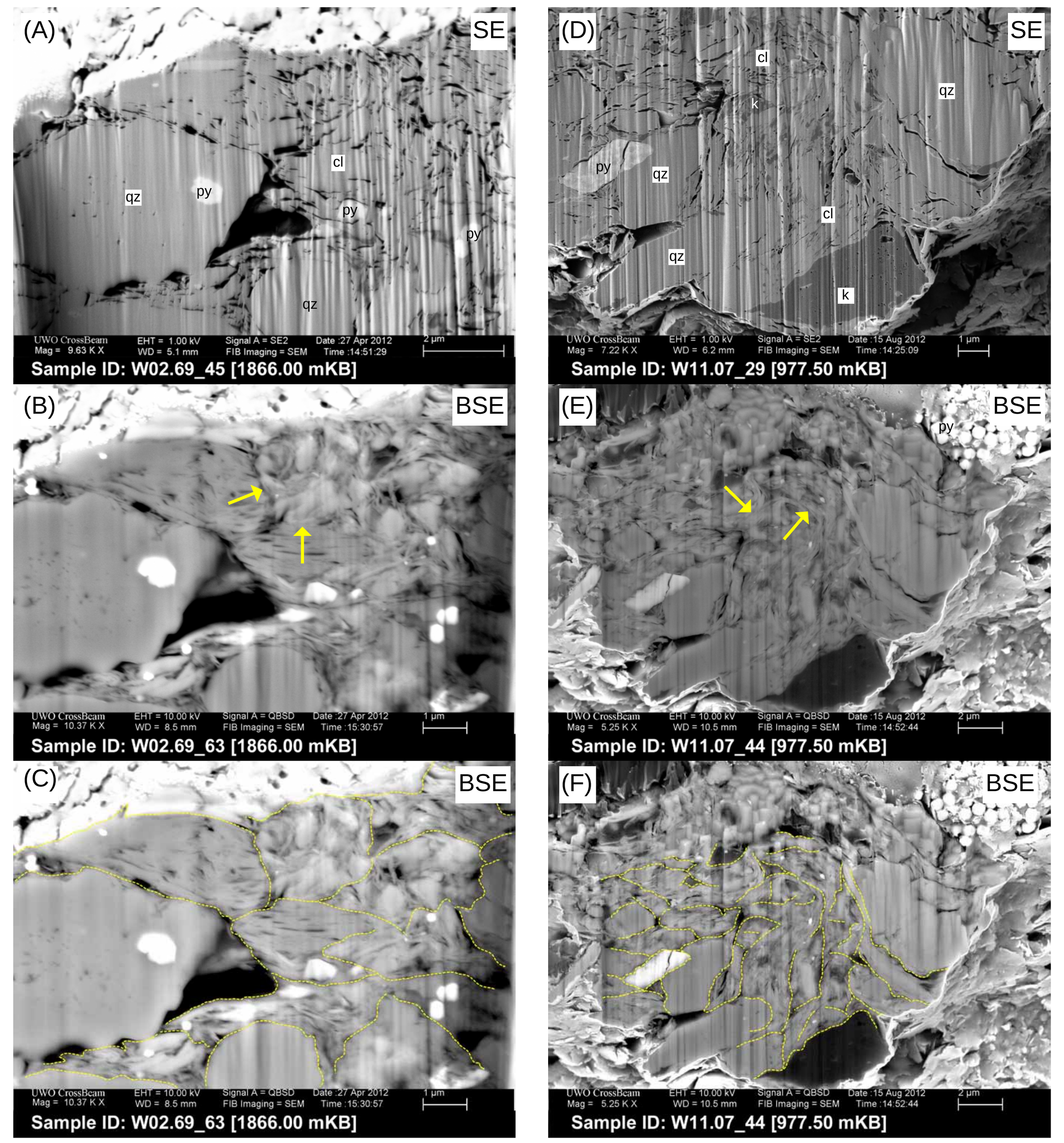

Figure 7.2. Two examples of clay aggregate microfabrics preserved in Lower Colorado Group carbonaceous mudstones. Figures (A) through (C) are from a sample of the Upper Belle Fourche Alloformation in a thermally mature (Tmax = 448° C) proximal foredeep setting. Figure (D) through (F) are from the Lower Belle Fourche Alloformation in the thermally immature (Tmax = 420° C) backbulge segment of the WCFB. The two samples have experienced significantly different burial histories. In both cases, the succession of FIB-SEM images begins with a secondary electron (SE) image, followed by an uninterpreted and interpreted backscatter (BSE) image. The backscatter images reveal the internal alignment of clay platelets within the aggregate microfabric. The indicated mineralogies in the SE images are quartz (qz), clay (cl), pyrite (py), and kerogen (k).

In sample W02.69, figures (B) and (C), discrete domains of clay platelet orientation are clearly evident. The yellow arrows in (B) show examples of boundaries between discrete domains, outlines of which are interpreted in yellow dashed lines in (C). These domains are interpreted as individual clay floccule particles (flocs or microflocs) which have subsequently aggregated with other flocs to produce aggregate grains. One remarkable feature of the interpretation in (C) is the fact that the individual flocs have largely retained equant aspects despite significant burial-related compaction. Consequently, the preservation potential of intraparticle porosity within the flocs is observed to be relatively high in samples that have experienced maximum burial in excess of 2000 metres.

The FIB-SEM images from sample W11.07 illustrate the characteristics of preserved organominerallic aggregates (Macquaker et al., 2010) which exhibit the aggregate microfabric described previously, but also incorporate a large proportion of kerogen (dark grey regions within flocs) in an intimate admixture between clay platelets. The large amorphous kerogen maceral in the lower central region of the image is interpreted to be independent of the deformed OMA particle.

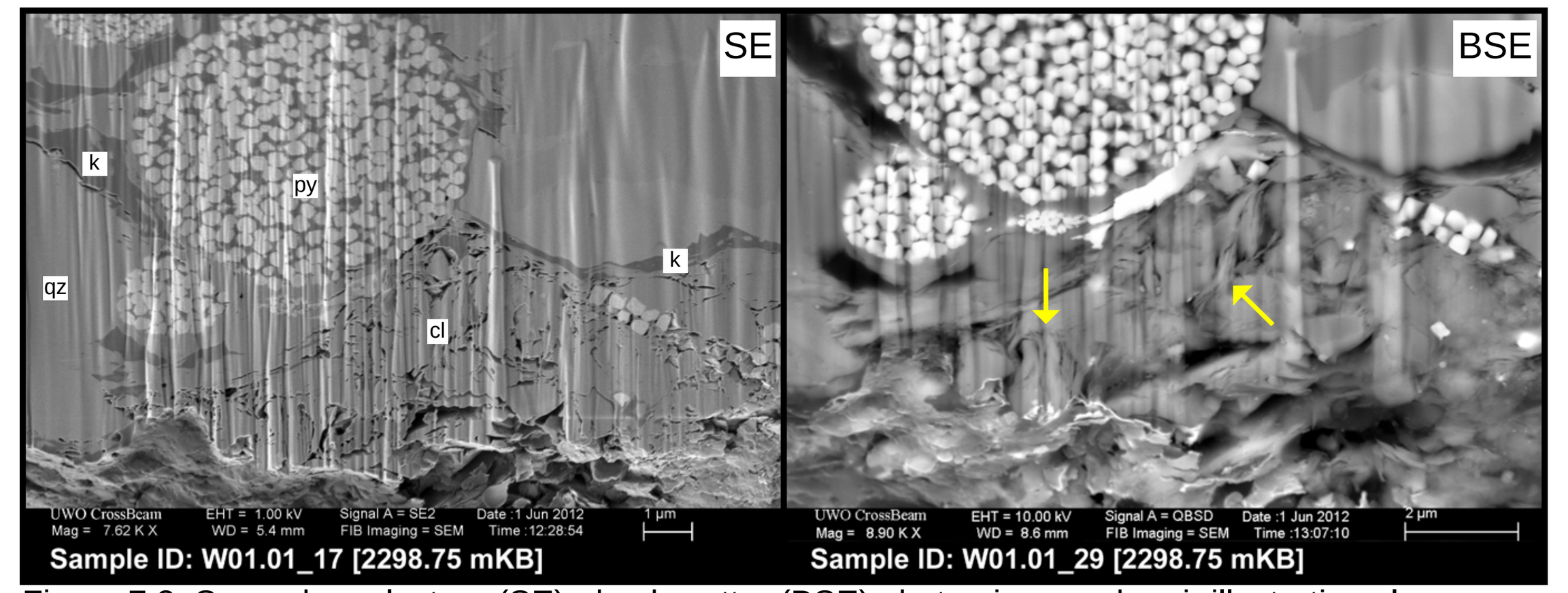

Figure 7.3. Secondary electron (SE) - backscatter (BSE) photomicrograph pair illustrating clay aggregate microfabric in a proximal foredeep location. The yellow arrows in the BSE image indicate edge-face contacts between clay platelets.

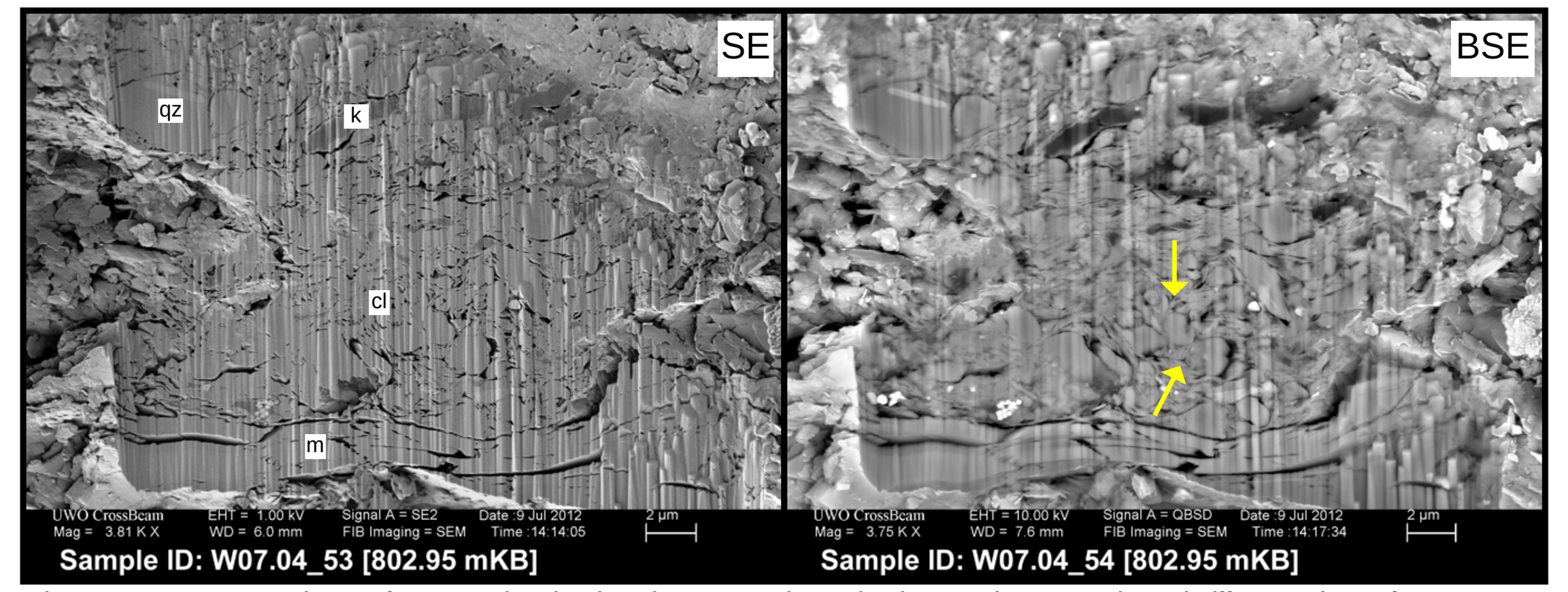

Figure 7.4. Secondary electron (SE) - backscatter (BSE) photomicrograph pair illustrating clay aggregate microfabric in a distal foredeep location. The yellow arrows in the BSE image indicate triangular intraparticle pores. The mica flake (m) is unrelated to the aggregate particle.

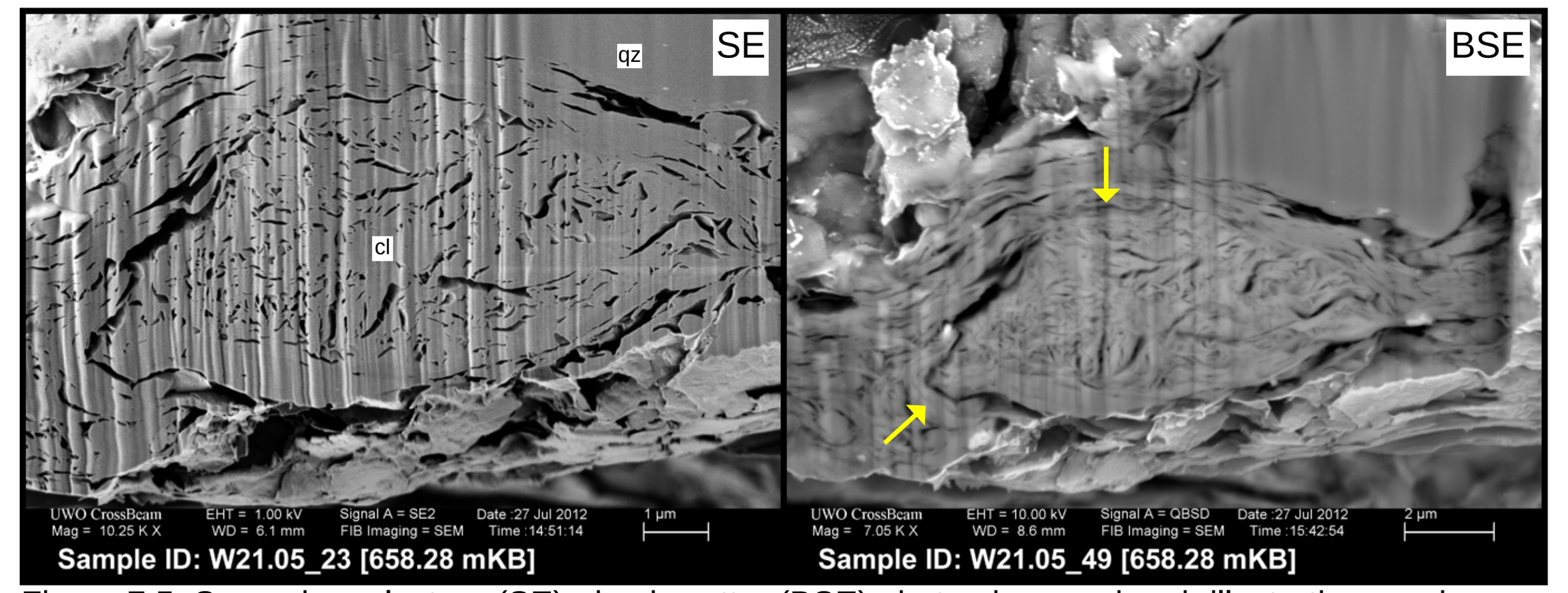

Figure 7.5. Secondary electron (SE) - backscatter (BSE) photomicrograph pair illustrating a unique clay aggregate microfabric in a distal foredeep location. The yellow arrows in the BSE image indicate how surrounding clay platelets enveloped this particle indicating it was competent during deposition.

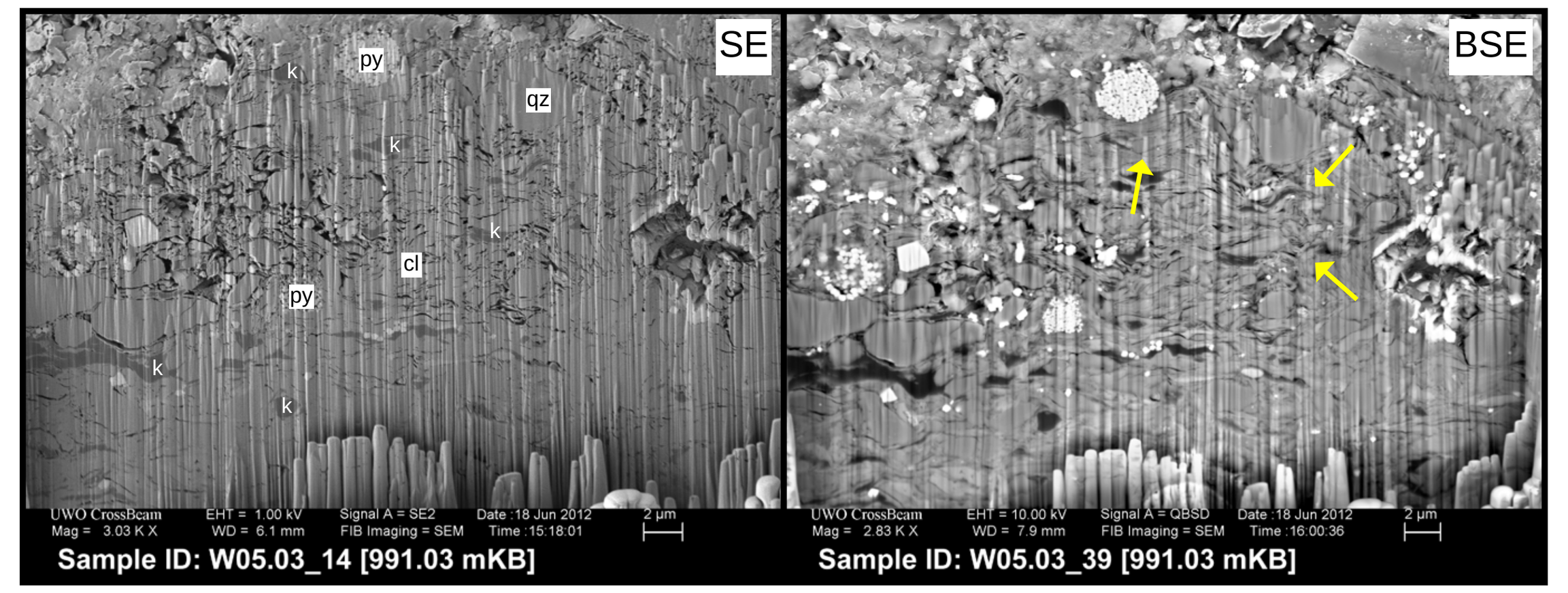

Figure 7.6. Secondary electron (SE) - backscatter (BSE) photomicrograph pair illustrating organominerallic aggregate microfabric in a distal foredeep location. The yellow arrows in the BSE image indicate internal domain boundaries.

8. Qualitative Observations

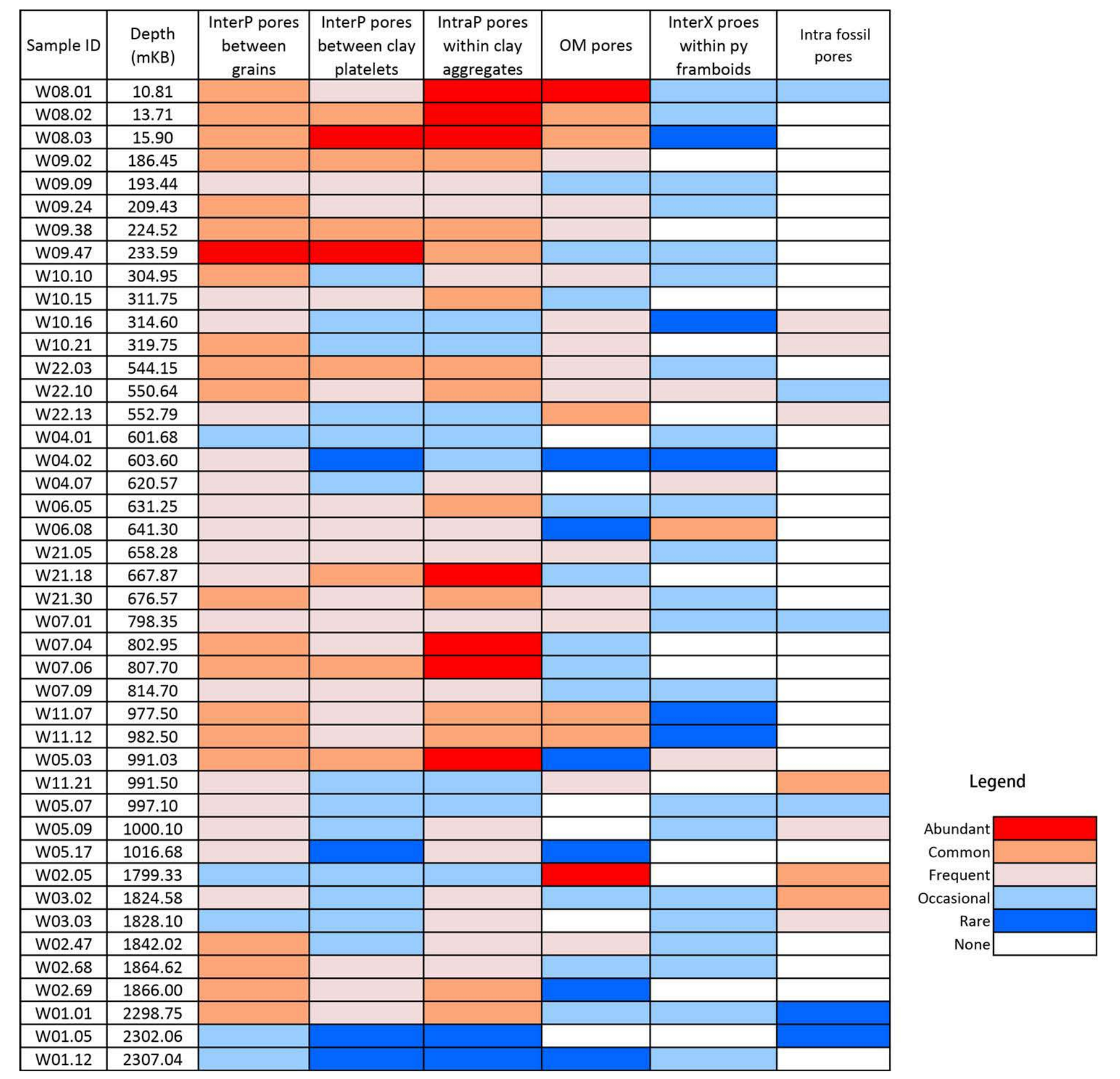

Figure 8.1. Qualitative evaluation of the relative abundance of the dominant modes of microporosity in Lower Colorado Group samples in this study. The samples have been listed in order of increasing depth. Note that post-Laramide uplift has reduced all of these depths from their maximum burial depths, so that the current values are only representative of the probable extent of burial-related compaction. A related PhD research project is currently developing 2-D burial history transects, and will evaluate compaction in a more quantitative fashion.

The relative abundance of the tabulated microporosity modes was determined by visual inspection of FIB-SEM images from multiple ion-milled surfaces for each sample. The subjective determination of relative abundance is indicated by the color scheme that ranges from cool to hot colors with increasing frequency of occurence. A future research project will use image analysis of classified and calibrated photomicrographs to produce objective quantitative data suitable for statistical analysis.

Within the limitations of this qualitative assessment, two observations may be inferred with reasonable certainty. The first is that the diversity of microporosity modes is relatively high for almost all of the samples, regardless of depth. A high proportion of samples have at least two distinct micropore modes that are rated as “common” or “abundant”. This reflects the “hybrid” nature of the Lower Colorado Group carbonaceous mudstone reservoirs, which incorporate granular quartz (silt and very fine sand), clays and clay aggregates, carbonate allochems, and diseminated organic matter.

The second observation is that porosity is preserved at the “frequent” or better level of abundance for the majority of samples, regardless of depth. The observed modes of microporosity are surprisingly resistant to compactional destruction, at least within the depth range sampled for this study.

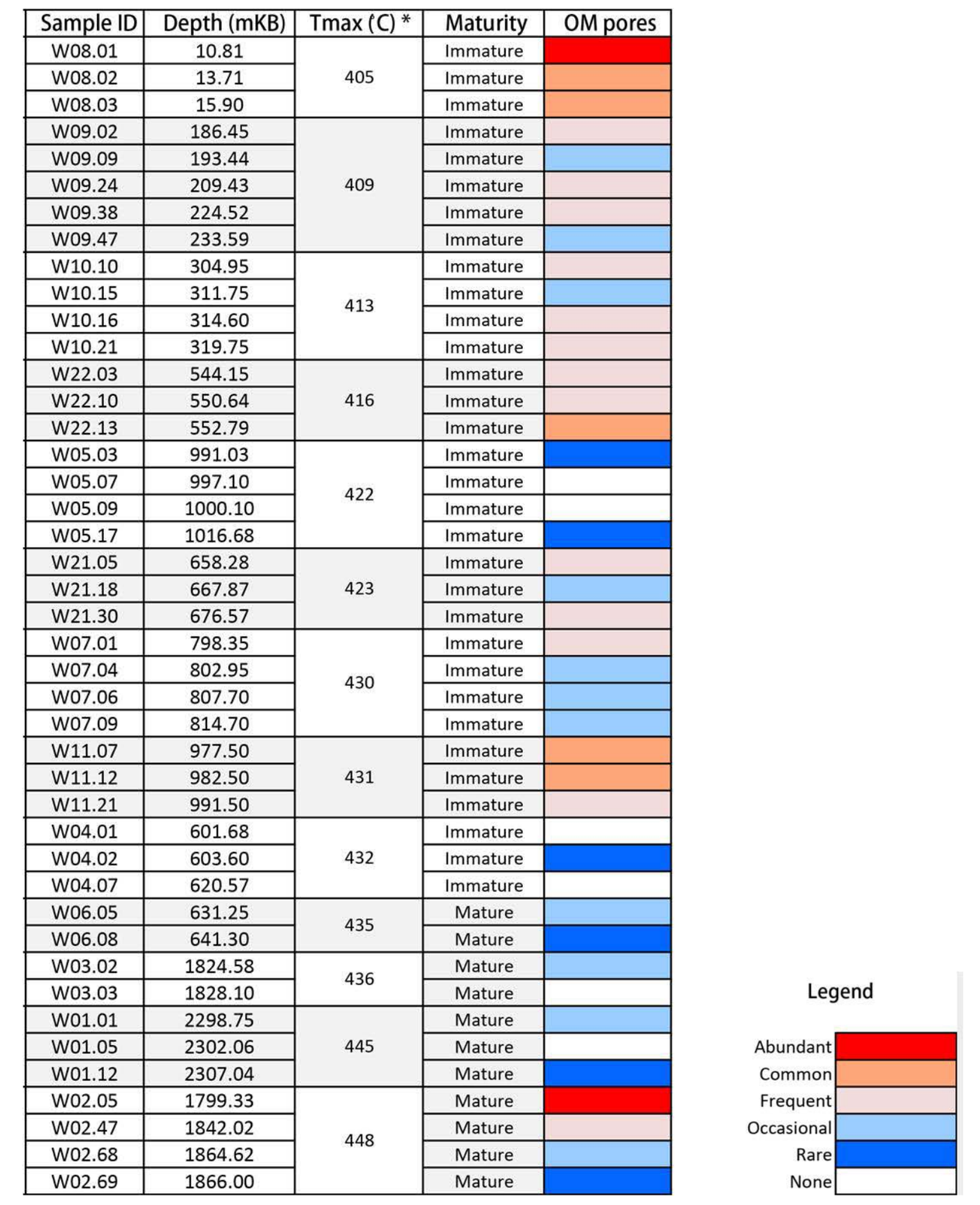

Figure 8.2. Qualitative evaluation of the relative abundance of the organic matter (OM) microporosity in Lower Colorado Group samples in this study. The samples have been listed in order of increasing thermal maturity using Rock-Eval Tmax as a proxy. Tmax was determined explicitly for locations W02, W09 and W10 as part of a regional Rock-Eval 6 analysis suite for this study. Tmax was estimated for the other locations based on maps constructed using public domain legacy data from 116 wells in the WCFB.

As above (Figure 8.1), the relative abundance of OM microporosity was determined by visual inspection of FIB-SEM images from multiple ion-milled surfaces for each sample. The subjective determination of relative abundance is indicated by the color scheme that ranges from cool to hot colors with increasing frequency of occurence. This represents an average degree of micropore development from a population of OM macerals for each sample. However, it is important to note that the variance of intraparticle OM microporosity within any given sample, which has not been quantified in this study, can be high due to the variation in susceptibility of different kerogen types to either microbial or thermogenic porositization pathways.

Notwithstanding the limitations of this qualitative assessment method, our observations provide visual evidence that OM microporosity in the Lower Colorado Group does not increase with increasing thermal maturity. The greatest abundance is associated with thermally immature samples from the backbulge segment of the basin. In part, this reflects the preferential organic enrichment in the backbulge where average TOC typically exceeds 5%, compared to 2% or less in the foredeep. Moreover, the high abundance of OM microporosity in the backbulge probably results from microbial consumption associated with the widespread occurence of biogenic gas in the shallow Cretaceous of the WCFB (Shurr and Ridgley, 2002).

9. Discussion

The observations presented in this poster represent a progress report, and a significant amount of work remains to validate our working hypotheses and develop a robust model that may be used to assess reservoir risk and predict optimal completion targets for oil and natural gas resources associated with the Second White Specks play.

The stratigraphic and depositional context of the images we present is not explicitly examined in this presentation, but it is an essential element of the approach we are taking to develop a process-based model that spans the current gap between petroleum systems modeling and reservoir characterization. Currently, a parallel PhD project is developing a basinwide high-resolution allostratigraphic framework that will provide that all-important context.

Similarly, our understanding of the relationship between porosity preservation and compaction remains inferential, at best, until we complete the construction of 2-D and 3-D burial history transects that will provide insight into the linkage (or lack thereof?) of subsidence and uplift hisotries between the foredeep, forebulge and backbulge segments of the WCFB during the Upper Cretaceous.

The nature of redistribution of mud within the shallow ramp depositional setting of the northern Western Interior Seaway remains enigmatic. Our observations show us that clay (and associated organic matter) has been “repackaged” and transported as aggregate grains. However, we do not have any direct evidence for either the distance or paleocurrent orientation associated with this sediment transport in the backbulge, several hundreds of kilometres from the shorelines of the foredeep segment. Future work will attempt to use a combination of oriented samples from outcrop and geochemical methods to begin to resolve this question.

We have interpreted the common development of OM microporosity in the backbulge basin as the result of microbial degeneration. However, we do not yet have direct evidence of this pathway to porosity development, nor do we know the timing of such a mechanism. Furthermore, if it is determined that OM microporosity is an early phenomenon then we are faced with the question of the fate of these pores with subsequent burial. If they are preserved in the thermogenic window, do they influence the progress of catagenic degradation of kerogen and attendant thermogenic porosity development?

10. Conclusions

One theme that is emerging at this early stage of investigation is the realization that microfabric analysis based on FIB-SEM imaging and related forms of microscopy provides essential visual evidence of the depositional processes that imprint the fundamental characteristics of reservoir quality in self-sourcing, carbonaceous mudstone reservoirs (i.e.: “source-reservoirs”). The diminutive size of the micropores that constitute the bulk of the storage capacity of these reservoirs neccesitates observations at the sub-micron scale.

Our preliminary observations indicate that most of the microporosity in the “hybrid” source-reservoirs of the Lower Colorado Group is inherited at the time of deposition as a result of the advective transport of fluid muds and silt-sized organominerallic aggregates. The formation of these aggregates, in turn, potentially accounts for the preservation of reactive (pyrolysable) carbon. Previous work demonstrated the effectiveness of the formation of “marine snow” as a mechanism to encapsulate disseminated organic matter in a micro reducing environment that prevents mineralization (Macquaker et al., 2010).

The visual evidence indicates that aggregate grains are surprisingly resilient, resisting compactional porosity loss to maximum burial depths of at least 2000 metres. This suggests that they may consolidate into mechanically strong grains at a very early stage following formation. This is important because it implies that intraparticle microporosity of aggregate grains, which appears to be established at the time of deposition, is redistributed by bottom currents in a manner analogous to the transport of other granular clastic grains such as silt. Indeed, the presence of very fine silt is virtually ubiquitous in our sample suite, and is commonly associated with clay aggregate microfabrics.

Our current understanding of clastic sequence stratigraphy is largely predicated on the understanding that the magnitude and rate of accommodation change (driven by the interplay of subsidence, eustacy and sediment supply) is the principal agent governing clastic stratal successions. Is it possible, therefore, that the accommodation principle that affords prediction of sandstone and siltstone distribution in a chronostratigraphic framework may also be applied to the abundant microporosity entrained in clay aggregate grains?

References

Aplin, A.C., and Macquaker, J.H., 2011, Mudstone diversity: Origin and implications for source, seal, and reservoir properties in petroleum systems: AAPG Bulletin, 95, 2031-2059.

Bloch, J., C. Schröder-Adams, D. Leckie, D. McIntyre, J. Craig, and M. Staniland, 1993, Revised stratigraphy of the lower Colorado Group (Albian to Turonian), western Canada: Bulletin of Canadian Petroleum Geology, 41, 325-348.

Loucks, R. G., R. M. Reed, S. C. Ruppel, and U. Hammes, 2012, Spectrum of pore types and networks in mudrocks and a descriptive classification for matrix-related mudrock pores: AAPG Bulletin, v. 96, p. 1071-1098.

Macquaker, H.S., Keller, M.A., and Davies, S.J., 2010, Algal blooms and “marine snow”: Mechanisms that enhance preservation of organic carbon in ancient fine-grained sediments: Journal of Sedimentary Research, 80, 934-942.

Nishida, N., M. Ito, A. Inoue, and S. Takizawa, 2013, Clay fabric of fluid-mud deposits from laboratory and field observations: Potential application to the stratigraphic record: Marine Geology, 337, 1-8.

Plint, A. G., J. H. Macquaker, and B. L. Varban, 2012, Bedload Transport of Mud Across A Wide, Storm-Influenced Ramp: Cenomanian–Turonian Kaskapau Formation, Western Canada Foreland Basin: Journal of Sedimentary Research, v. 82, p. 801-822.

Shurr, G. W., and J. L. Ridgley, 2002, Unconventional shallow biogenic gas systems: AAPG Bulletin, v. 86, p. 1939-1969.

Talling, P. J., D. G. Masson, E. J. Sumner, and G. Malgesini, 2012, Subaqueous sediment density flows: Depositional processes and deposit types: Sedimentology, v. 59, p. 1937-2003.

Tyagi, A., A. G. Plint, and D. H. McNeil, 2007, Correlation of physical surfaces, bentonites, and biozones in the Cretaceous Colorado Group from the Alberta Foothills to southwest Saskatchewan, and a revision of the Belle Fourche - Second White Specks formational boundary: Canadian Journal of Earth Sciences, v. 44, p. 871-888.

Acknowledgements

Funding for this work is provided by Husky Energy Inc., Devon Energy Corporation, and Tuzo Energy Corporation through their membership in the Second White Specks Liquids-Rich Research Consortium.

Imaging work was conducted in the Western Nanofabrication Facility at Western University in London, Ontario, Canada.

The authors also acknowledge the generous support of Schlumberger, geoLOGIC Systems Ltd., Divestco Inc., and IHS (Canada) Limited who donated software and data products used in this research.